# Robust Coherent Transport of Light in Multilevel Hot Atomic Vapors

N. Cherroret, M. Hemmerling, V. Nador, J T M Walraven, R. Kaiser

# Robust coherent transport of light in multi-level hot atomic vapors

N. Cherroret,[1] M. Hemmerling,[2,3] V. Nador,[3] J.T.M. Walraven,[4] and R. Kaiser[3]

[1] *Laboratoire Kastler Brossel, Sorbonne Université, CNRS, ENS-PSL University, Collège de France; 4 Place Jussieu, 75005 Paris, France*
[2] *Instituto de Física de São Carlos, Universidade de São Paulo, 13560-970 São Carlos, SP, Brazil*
[3] *Université Côte d'Azur, CNRS, Institut de Physique de Nice, Valbonne F-06560, France*
[4] *Van der Waals-Zeeman Institute, Institute of Physics, University of Amsterdam, Science Park 904, 1098 XH Amsterdam, The Netherlands*

Using a model system, we demonstrate both experimentally and theoretically that coherent scattering of light can be robust in hot atomic vapors despite a significant Doppler effect. By operating in a linear regime of far-detuned light scattering, we also unveil the emergence of interference triggered by inelastic Stokes and anti-Stokes transitions involving the atomic hyperfine structure.

Coherent transport in disordered media is at the focus of intense investigations in many fields of research, including condensed matter [1], astrophysics [2], acoustics [3], optics [4], atomic physics [5] and ultracold atoms [6]. In these fields, many coherence related phenomena are often not fully controlled and described by effective parameters. In particular, treatments of light propagation in atomic vapors often leave aside the internal atomic structure and use a simplified two-level model. Interestingly, in cases when the detailed structure is accounted for, not only the quantitative description is improved, but new qualitative features emerge, such as Sisyphus cooling [7], slow light [8] and quantum memories [9]. Another ingredient adding to the complexity of light propagation in these systems is Doppler broadening. With the impressive improvement of high-precision measurements allowed by the development of atom laser cooling, a fine, microscopic description of temperature effects has become crucial. A well known example are collective phenomena in nearby coupled dipoles [10–15] which involve Doppler-sensitive interference. This question is also central in room temperature atomic vapors, which have seen a renewed interest in precision measurements, including applications on electric-field sensors [17] and quantum information [18–21]. In hot vapors, it is commonly thought that interference are washed out by Doppler broadening and a radiative transfer equation is often used as a simplified model [5]. This description, however, misses many intriguing phenomena like collective lamb shifts [15] or the polarization anomaly at the D1 line of the solar spectrum [16]. In this Letter, we show that thermal decoherence in hot atomic vapors can be largely circumvented by operating in the large detuning limit where atomic motion is negligible during scattering events. In this regime, we also discover that the multi-level atomic structure leads to a new interference mechanism based on inelastic Raman scattering from hyperfine levels, which we describe with a quantitatively accurate microscopic theory.

Our experiment is sketched in Fig. 1. A collimated laser beam (waist $w = 10$ mm) is sent through a slab-shaped glass cell containing a natural mixture of rubidium vapor at an oven-regulated temperature/density. The wavelength $\lambda = 780$ nm is set to the D2 transition of rubidium. Two cells were used, one with a metallic mirror clipped to the back side, and another one without such a mirror. The angle of incidence of the laser beam, $\theta_0 \ll 1$, was adjusted to typically a few tens of milliradians with respect to the surface normal of the slab. The backscattered light was observed in the far field with an optical angular resolution of 0.044 mrad using a CCD camera (Fig. 1). Due to light scattering, this signal has generically two types of contributions: the "incoherent" ones, associated with in-phase pairs of paths traveling along an identical sequence of scatterers, and the "coherent" ones where the two paths accumulate a finite phase difference [22]. In the multiple scattering regime the latter leads in particular to the coherent backscattering effect, which was previously measured in cold atomic gases [23]. Our goal is to investigate the coherent component of the signal in a hot vapor. For this purpose, the cell is heated to temperatures on the order of 200°C.

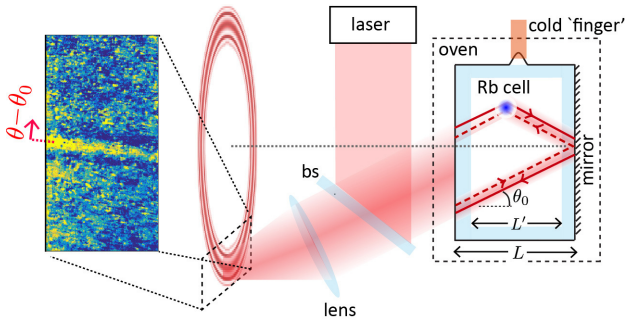


FIG. 1: (Color online) Experimental scheme (for clarity polarization elements are not shown). A collimated laser beam is sent via a beamspitter (bs) through a glass cell (width $L \simeq 8$ mm, chamber thickness $L' \simeq 6$ mm) containing a hot rubidium mixture. An oven with a cold 'finger' is used to regulate the vapor pressure in the cell. The backscattered signal is collected in the far field on a CCD camera. In the cell, the interference between counter-propagating wave paths scattered on both an atom and the back face of the cell gives rise to annular fringes ("mirror-assisted coherent backscattering").

In this regime, the atomic motion is very fast which a priori constitutes an unfavorable case for coherent transport. Indeed, the Doppler effect associated with thermal motion induces a random frequency shift in scattered wave paths, a phase-breaking mechanism usually detrimental to interference [24, 25]. To counteract this mechanism, our strategy has been to operate at large detuning $|\Delta \equiv \omega - \omega_0| \gg k\overline{v}$ so that the characteristic time $\sim \lambda/\overline{v}$ for an atom to move over a wavelength becomes much longer than the time $\tau \sim \Gamma^{-1}(\Gamma/\Delta)^2$ of a scattering process ($\omega$ and $\omega_0$ are the laser and atomic angular frequencies, $\Gamma$ is the natural linewidth, $k = 2\pi/\lambda$ is the wave number and $\overline{v} = \sqrt{k_B T/m}$ is a measure for the atomic thermal speed). The left panel of Fig. 1 shows a typical experimental CCD image, obtained at $T \simeq 195°$C and $|\Delta| = 2$ GHz [26, 27]. Under these conditions, $|\Delta|/k\overline{v} \simeq 7.3 \gg 1$ and $k\overline{v}/\Gamma \simeq 45 \gg 1$. Despite the large Doppler effect, the image in Fig. 1 displays a well contrasted interference fringe, suggesting that atoms effectively behave like cold ones. This fringe stems from the interference between counter-propagating wave paths scattered on both an atom and the mirror on the back face of the cell, as illustrated in Fig. 1. It leads to an interference ring known as the "mirror-assisted coherent backscattering" (mCBS) effect [28–30], on which we will concentrate our attention from now on. While mCBS was recently measured in a cold Strontium gas [30], its visibility in a *hot* rubidium vapor with highly nontrivial quantum-level structure is far from obvious. To understand it, we have analytically calculated the enhancement factor $\Lambda \equiv (S_b + S_{\rm mCBS})/S_b$ of the mCBS signal $S_{\rm mCBS}$ with respect to the incoherent background signal $S_b$, taking into account the thermal distribution of atomic velocities, see Supplemental Material (SM):

$$\Lambda(\theta, T) = 1 + \Lambda_0 \exp\left[-2\left(\frac{k\overline{v}\theta_0 L}{\Gamma\ell}\right)^2\right] \times \cos[kL(\theta-\theta_0)\theta_0]\mathrm{sinc}[kL'(\theta-\theta_0)\theta_0], \quad (1)$$

where $\theta - \theta_0$ is the angular deviation from the fringe maximum, see Fig. 1, and $\Lambda_0 \equiv \Lambda(\theta_0, T = 0) - 1$. Eq. (1) indeed describes an interference ring, with radial oscillations governed by two length scales, the distance $L/2$ from the center of the cell to the mirror, and the thickness $L'$ of the vapor [30]. The exponential factor stems from the thermal average of the dephasing $e^{i\Delta\Phi_T}$ accumulated by the two interfering paths, whose frequency is Doppler shifted by $\boldsymbol{v}\cdot\Delta\boldsymbol{k}$ upon scattering with momentum change $\Delta\boldsymbol{k}$ on an atom of velocity $\boldsymbol{v}$:

$$\Delta\Phi_T \sim L\boldsymbol{v}\cdot\Delta\boldsymbol{k}\,\frac{\partial k}{\partial\omega} \sim \frac{Lk\overline{v}\theta_0}{\Gamma\ell}, \quad (2)$$

where we used that $\partial k/\partial\omega \sim 1/\Gamma\ell$ when $|\Delta| \gg \Gamma$, with $\ell$ the mean free path. Eq. (2) explains the robustness of the mCBS interference against thermal motion. First, since $|\Delta| \gg k\overline{v}$ we have $\ell \simeq \ell(\overline{v} = 0) \propto k^2\rho^{-1}(\Delta/\Gamma)^2$, where $\rho$ is the atom density. The impact of dephasing is thus lessened at large detuning. The second reason lies in the proportionality of $\Delta\Phi_T$ to the incident angle $\theta_0 \ll 1$: as we operate near normal incidence, scattering is essentially forward ($\Delta\boldsymbol{k} \sim 0$) which again reduces $\Delta\Phi_T$. Fig. 2 shows a typical experimental angular profile $\Lambda(\theta, T)$ of the mCBS ring (blue dots). To obtain these data, we have measured both the background $S_b$ and mCBS $S_{\rm mCBS}$ signals from which we have removed stray light by subtracting the signal at $|\Delta| = 40$ GHz. The profile is compared with Eq. (1), shown as a solid red curve. For this comparison, the amplitude at $\theta = \theta_0$, $\Lambda(\theta_0, T)$, is set to the experimental value 1.20. Except for this reference point though, there is no adjustable parameter: the agreement for the width of the central fringe and even for the first secondary fringes is excellent.

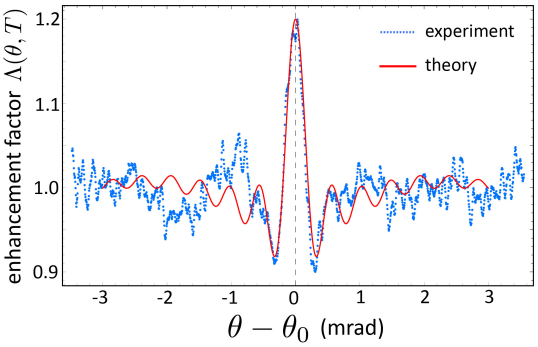


FIG. 2: (Color online) Angular radial cut of the mCBS interference ring (detuning $|\Delta| = 2$ GHz, incident angle $\theta_0 \simeq 7°$, polarization channel $h \perp h$). Blue dots are the experimental signal. The red curve is Eq. (1) in which the amplitude at $\theta = \theta_0$, $\Lambda(\theta_0, T)$, is set to the experimental value 1.20. Except for this reference point, there is no adjustable parameter.

The most interesting property of Eq. (2) is the dependence of $\Delta\Phi_T$ on the mean free path $\ell \propto (\Delta/\Gamma)^2$. This offers the possibility to turn from a hot to a cold atom behavior in a controlled way via a change of the detuning. To check this property, we have measured the mCBS enhancement factor $\Lambda(\theta = \theta_0, T)$ as a function of $|\Delta|$ over a broad range. The results are presented in Fig. 3. The curves correspond to three detection schemes where linearly polarized light is analyzed along the parallel ($l \parallel l$) or perpendicular ($l \perp l$) channels, or where circularly polarized light is analyzed in the channel of opposite ($h \perp h$) helicity [23, 31], as routinely done in experiments on light scattering in random media. No signal is observed in the channel $h \parallel h$ because at large detuning the excited hyperfine levels of the D2 line of rubidium are not resolved so that the single scattering process is essentially equivalent to a $J = 1/2 \to 3/2$ transition [32]. Let us first discuss the variation of the curves with detuning. We attribute it to the exponential factor in Eq. (1). Fits of the experimental data to Eq. (1) (solid curves in Fig. 3) validate this interpretation and demonstrate our ability to

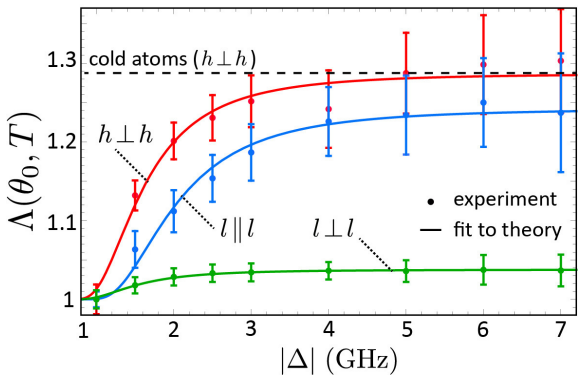


FIG. 3: (Color online) mCBS enhancement factor $\Lambda(\theta_0, T)$ as a function of detuning in three polarization channels. The experimental data (dots) are fitted with Eq. (1) at $\theta = \theta_0$, using $\Lambda_0$ and $\rho k^{-3}$ as fit parameters (solid curves). These fits provide $\rho k^{-3} = 0.15$, 0.22, 0.14 and $\Lambda_0 = 0.038$, 0.242 and 0.287 in the channels $l \perp l$, $l \parallel l$ and $h \perp h$, respectively. No signal is observed in the channel $h \parallel h$. The dashed line shows the enhancement factor expected for cold atoms (i.e. in the limit $k\bar{v}/\Gamma \to 0$) in the channel $h \perp h$.

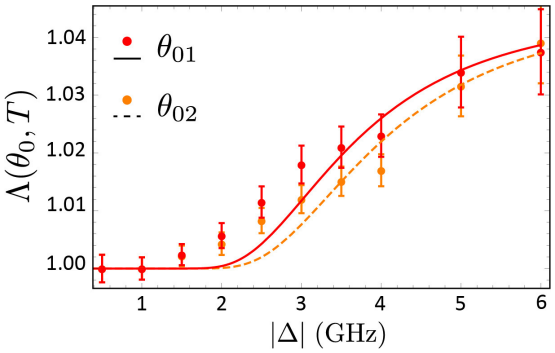


FIG. 4: (Color online) mCBS enhancement factor $\Lambda(\theta_0, T)$ versus detuning at two incident angles $\theta_0 = \theta_{01}$ and $\theta_{02} > \theta_{01}$, in the channel $h \perp h$ at fixed $T \simeq 168°$. Dots are experimental points and curves are fits to Eq. (1).

control the thermal dephasing via the detuning in the vapor. For comparison, in the channel $h \perp h$ we also show as a dashed line the enhancement $\Lambda(\theta_0, T = 0) = 1 + \Lambda_0$ expected for cold atoms. In fact, Fig. 3 indicates that the "cold atom limit" is almost reached for $\Delta \gtrsim 4$GHz whatever the polarization configuration.

For the fits to Eq. (1), we use $\Lambda_0$ and $\rho k^{-3}$ as free parameters and extract a nearly constant parameter $\rho k^{-3} = 0.17 \pm 0.05$, which confirms the independence of the dephasing (2) upon polarization. The relative values of enhancement factors in the various polarization channels thus stem from the zero-temperature amplitude $\Lambda_0 = S_{\rm mCBS}/S_b$. We attribute it to the proportionality of the mCBS signal $S_{\rm mCBS}(T = 0)$ to the elastic differential cross-section $d\sigma_{\rm el}/d\Omega$, assuming that the background signal $S_b(T = 0)$ is independent of polarization. Except at low detuning this assumption is approximately verified in our setup. For an incident wave whose polarization vector changes from $\boldsymbol{\epsilon}_{\rm in}$ to $\boldsymbol{\epsilon}_{\rm out}$ upon scattering on an atom, it was shown, based on the decomposition of the scattered intensity into irreducible components with respect to the rotation group, that $d\sigma_{\rm el}/d\Omega \propto w_1|\boldsymbol{\epsilon}_{\rm in} \cdot \boldsymbol{\epsilon}^*_{\rm out}|^2 + w_2|\boldsymbol{\epsilon}_{\rm in} \cdot \boldsymbol{\epsilon}_{\rm out}|^2 + w_3$ [33, 34]. The numerical coefficients $w_i$ depend on the fine and hyperfine level structure of rubidium. We have calculated them using the approach developed in [32] for treating light scattering from hyperfine multiplets. From this calculation we evaluate the ratios $\Lambda_0(h \perp h)/\Lambda_0(l \parallel l) \simeq 1.1$ and $\Lambda_0(l \parallel l)/\Lambda_0(l \perp l) \simeq 8.0$ [35], in reasonable agreement with the experimental ratios extracted from the fits in Fig. 3: $\Lambda_0^{\rm exp}(h \perp h)/\Lambda_0^{\rm exp}(l \parallel l) \simeq 1.2$ and $\Lambda_0^{\rm exp}(l \parallel l)/\Lambda_0^{\rm exp}(l \perp l) \simeq 6.4$.

According to Eq. (1), the thermal dephasing (2) can be also controlled with the incident angle $\theta_0$. To verify this property, we have measured the mCBS enhancement factor as a function of detuning for two different angles $\theta_{01} \simeq 6.5°$ and $\theta_{02} \simeq 7.5° > \theta_{01}$ deduced from the mCBS angular profiles. These measurements are displayed in Fig. 4 (dots). We fit them with Eq. (1) with $\Lambda_0$ as a single fit parameter (solid and dashed curves), inferring the atom density $\rho$ from the saturated vapor pressure in the cell. For these measurements we used another atomic cell heated to $T \simeq 168°$ and on which no mirror was clipped on the back face (the glass itself thus plays the role of the mirror). $\Lambda_0$ being also proportional to the reflection coefficient of the glass [30], much smaller than the one of the mirror, this leads to smaller enhancement factors than in Fig. 3.

In the description of the mCBS interference presented so far, we implicitly assumed that light was scattered *elastically* on the atom (Rayleigh scattering). As we operate at a large detuning $|\Delta| \gg \Gamma$ though, the light-matter interaction may involve atomic transitions where several hyperfine levels come into play, such that it is not guaranteed that only Rayleigh scattering occurs. A quick look at the typical level structure of rubidium, recalled in Fig. 5(b), confirms this statement: the structure involves two ground-state levels $F$ and $F + 1$, the various Zeeman sub-levels of which are equally populated in our hot vapor. When subjected to light, atoms may experience Rayleigh transitions $F \to F$ or $F + 1 \to F + 1$ via any of the allowed excited levels [the Rayleigh transition $F + 1 \to F + 1$ is illustrated in Fig. 5(b)]. These processes, whose strength is encapsulated in the elastic scattering cross-section, yield the elastic mCBS ring discussed previously. Since $\Delta$ is large compared to the typical spacing between the excited hyperfine levels, those are not resolved in our experiment. $\Delta$ is, on the other hand, *not* small compared to the spacing $\Delta_0$ between the two ground-state levels $F$ and $F + 1$. This implies that Stokes ($F \to F + 1$) and anti-Stokes ($F + 1 \to F$) *inelastic* scattering processes can occur as well, see Fig.

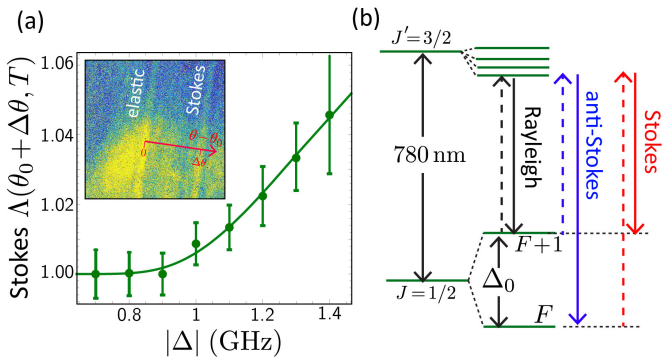


FIG. 5: (Color online) (a) Inset: CCD image showing a secondary mCBS ring associated with inelastic scattering, here visible in the channel $l \perp l$ at $|\Delta| = 1.3$ GHz. The red arrow is the $\theta - \theta_0$ axis; the secondary ring is maximum at $\theta = \Delta\theta + \theta_0$. Main panel: experimental enhancement factor $\Lambda(\theta = \theta_0 + \Delta\theta, T)$ of the secondary ring versus detuning (dots), together with a fit to Eq. (3). (b) Level structure of rubidium. In addition to elastic (Rayleigh) processes, at large detuning light can experience inelastic (Stokes and anti-Stokes) processes from the two ground-state levels separated by $\Delta_0$ [$\Delta_0 = 3.0$ GHz (6.8 GHz) and $F = 2$ ($F = 1$) for $^{85}$Rb ($^{87}$Rb)].

5(b). Note that this type of inelastic transitions here shows up in the *linear* regime of light scattering (small saturation parameter) and is thus fundamentally different from the inelastic processes that occur at higher intensities [36–39]. A refined analytical calculation of the mCBS effect (SM) shows that these Stokes/anti-Stokes transitions give rise to two *secondary* interference rings, of enhancement factor

$$\Lambda(\theta, T) = 1 + \Lambda_0 \exp\left[-2\left(\frac{k\bar{v}\theta_0 L}{\Gamma\ell}\right)^2\right] \times \cos[kL(\theta-\theta_0)\theta_0 + L\Delta k]\mathrm{sinc}[kL'(\theta-\theta_0)\theta_0 + L\Delta k]. \quad (3)$$

As compared to Eq. (1), an additional momentum shift $\Delta k$ arises because the light frequency changes by $\pm\Delta_0$ after Stokes or anti-Stokes scattering on the atom. This shift is given by

$$\Delta k = k\left[n(\Delta \pm \Delta_0) - n(\Delta)\right], \quad (4)$$

with a plus (minus) sign for the anti-Stokes (Stokes) process. In Eq. (4), $n$ is the refractive index of the gas. The momentum shift in Eq. (3) implies that inelastic rings are angularly separated by $\Delta\theta \simeq -\Delta k/(k\theta_0)$ from the elastic one. They are visible in polarization channels where inelastic scattering is present. We have found from calculations of inelastic scattering cross-sections that this is typically the case in the channel $l \perp l$, where we have experimentally focused our attention. In the inset of Fig. 5(a) we show a CCD image taken at $\Delta = -1.3$GHz and $T \simeq 166°$ in this channel: we indeed observe a secondary fringe close to the elastic one. To demonstrate that it is well of mCBS type, we have tested its sensitivity to thermal dephasing. The plot in Fig 5(a) confirms this sensitivity: the enhancement factor $\Lambda(\theta_0 + \Delta\theta, T)$ of the inelastic fringe versus $\Delta$ is well fitted by Eq. (3). From this fit we extract $\rho k^{-3} \simeq 0.16$, which we use to estimate the ring separation $\Delta\theta$. Assuming a Stokes process (a choice justified below) and estimating the refractive index for a dilute atomic cloud (SM), we find $\Delta\theta = 0.28°$ from Eq. (4) [40]. This value is on the order of the experimental one, $\Delta\theta_{\mathrm{exp}} = 0.15°$, measured on the camera image. A possible reason for the theoretical overestimation is the uncertainty on $\rho k^{-3}$. One may wonder, finally, why only one inelastic fringe is visible in the inset of Fig. 5, while Eq. (4) in principle predicts two fringes. The reason lies in the frequency asymmetry of the Stokes and anti-Stokes transitions. Indeed, unlike the Stokes process, the anti-Stokes process brings photons back to resonance [27]. This leads to a large momentum shift (4), which moves the anti-Stokes ring far away from the elastic one, out of the range of the camera [from Eq. (4) we estimate $\Delta\theta_{\text{anti-Stokes}} \sim -10\Delta\theta_{\text{Stokes}}$). Note that the Stokes nature of the secondary fringe in Fig 5(a) is also confirmed by its position with respect to the elastic one: for the Stokes process $n(\Delta - \Delta_0) - n(\Delta) < 0$ so that $\Delta\theta > 0$.

By operating at large detuning we have shown that elementary interference between optical paths can survive in hot atomic vapors. This finding could be exploited to enhance more complex interference phenomena under conditions of large Doppler effect, as well as collective interference effects like subradiance, so far only observed in cold gases [10]. We have also unveiled a novel interference mechanism based on inelastic scattering from hyperfine levels in the linear regime. This sheds light on the important role Raman processes might play in multiple scattering [41], a question yet largely unexplored in ensembles of quantum scatterers.

NC thanks Dominique Delande for helpful discussions, and financial support from and the Agence Nationale de la Recherche (grant ANR-14-CE26-0032 LOVE). This work was conducted within the framework of the project OPTIMAL granted by the European Union by means of the Fond Européen de développement régional, FEDER.

[1] E. Akkermans and G. Montambaux, *Mesoscopic physics of electrons and photons* (Cambridge university press, 2007).
[2] H. C. Van de Hulst, *Multiple light scattering: tables, formulas, and applications* (Elsevier, 2012).
[3] H. Hu, A. Strybulevych, J. Page, S. Skipetrov, and B. van Tiggelen, Nat. Phys. **4**, 945 (2008).
[4] S. Rotter and S. Gigan, Rev. Mod. Phys. **89**, 015005 (2017).
[5] A. F. Molisch and B. P. Oehry, *Radiation trapping in*

*atomic vapors, Clarendon Press*, Oxford (1998).
[6] A. Aspect and M. Inguscio, Physics today **62**, 30 (2009).
[7] J. Dalibard and C. Cohen-Tannoudji, J.O.S.A B **11**, 2043 (1989).
[8] L. V. Hau, S. E. Harris, Z. Dutton, and C. H. Behroozi, Nature, **397**, 6720 (1999).
[9] L. M. Duan, M. D. Lukin, J. I. Cirac, and P. Zoller, Nature **414**, 413 (2001).
[10] W. Guérin, M. O. Araùjo, and R. Kaiser, Phys. Rev. Lett. **116**, 083601 (2016).
[11] J. Pellegrino, R. Bourgain, S. Jennewein, Y. R. P. Sortais, A. Browaeys, S. D. Jenkins, and J. Ruostekoski, Phys. Rev. Lett. **113**, 133602 (2014).
[12] S. Jennewein, M. Besbes, N. J. Schilder, S. D. Jenkins, C. Sauvan, J. Ruostekoski, J.-J. Greffet, Y. R. P. Sortais, and A. Browaeys, Phys. Rev. Lett. **116**, 233601 (2016).
[13] L. Corman, J. L. Ville, R. Saint-Jalm, M. Aidelsburger, T. Bienaimé, S. Nascimbène, J. Dalibard, and J. Beugnon, Phys. Rev. A **96**, 053629 (2017).
[14] R. Saint-Jalm, M. Aidelsburger, J. L. Ville, L. Corman, Z. Hadzibabic, D. Delande, S. Nascimbène, N. Cherroret, J. Dalibard, and J. Beugnon, Phys. Rev. A **97**, 061801(R) (2018).
[15] T. Peyrot, Y. R. P. Sortais, A. Browaeys, A. Sargsyan, D. Sarkisyan, J. Keaveney, I. G. Hughes, and C. S. Adams, Phys. Rev. Lett. **12**, 243401 (2018).
[16] J. O. Stenflo, ApJ **801**, 70 (2015).
[17] J. Sedlacek, A. Schwettmann, H. Kübler, and J. Shaffer, Phys. Rev. Lett. **111**, 063001 (2013).
[18] A. Urvoy, F. Ripka, I. Lesanovsky, D. Booth, J. P. Shaffer, T. Pfau and R. Löw, Phys. Rev. Lett. **114**, 203002 (2015).
[19] D. J. Whiting, N. Sibalic, J. Keaveney, C. S. Adams, and I. G. Hughes, Phys. Rev. Lett. **118**, 253601 (2017).
[20] C. B. Moller, R. A.Thomas, G. Vasilakis, E. Zeuthen, Y. Tsaturyan, M. Balabas, K. Jensen, A. Schliesser, K. Hammerer, and E. S. Polzik, Nature **547**, 191 (2017).
[21] R. Jiménez-Martínez, J.Kolodynski, C. Troullinou, V. G. Lucivero, J. Kong, and M. W. Mitchell, Phys. Rev. Lett. **120**, 040503 (2018).
[22] P. Sheng, *Introduction to Wave Scattering, Localization, and Mesoscopic Phenomena, Academic Press, New York, (1995).*
[23] G. Labeyrie, F. de Tomasi, J.-C. Bernard, C. A. Müller, Ch. Miniatura and R. Kaiser, Phys. Rev. Lett. **83**, 5266 (1999).
[24] A. A. Golubentsev, Sov. Phys. JETP **59**, 26 (1984).
[25] G. Labeyrie, D. Delande, R. Kaiser, and C. Miniatura, Phys. Rev. Lett. **97**, 013004 (2006).
[26] Here and in the rest of the Letter, temperatures are given with an uncertainty of about 10° C.
[27] For convenience, in the experiment we choose to work with negative detunings.
[28] J.-J. Greffet, Waves Random Media **3**, S65 (1991).
[29] G. Labeyrie, C. A. Müller, D. S. Wiersma, C. Miniatura, and R Kaiser, J. Opt. B: Quant. Semiclass. Opt. **2**, 672 (2000).
[30] P. H. Moriya, R. F. Shiozaki, R. Celistrino Teixeira, C. E. Máximo, N. Piovella, R. Bachelard, R. Kaiser, and Ph. W. Courteille, Phys. Rev. A **94**, 053806 (2016).
[31] P. E. Wolf, G. Maret, E. Akkermans and R. Maynard, J. Phys. (France) **49**, 63 (1988).
[32] C. A. Müller, C. Miniatura, D. Wilkowski, R. Kaiser, and D. Delande, Phys. Rev. A **72**, 053405 (2005).
[33] A. Omont, Prog. Quantum Electron. **5**, 69 (1977).
[34] C. A. Müller and C. Miniatura, J. Phys. A **35**, 10163 (2002).
[35] N. Cherroret *et al.*, to be published.
[36] B. R. Mollow, Phys. Rev. **188**, 1969 (1969).
[37] T. Wellens, B. Grémaud, D. Delande, and C. Miniatura, Phys. Rev. A **70**, 023817 (2004).
[38] V. Shatokhin, C. A. Müller, and A. Buchleitner, Phys. Rev. Lett. **94**, 043603 (2005).
[39] T. Binninger, V. N. Shatokhin, A. Buchleitner, and T. Wellens, arXiv:1811.08882 (2018).
[40] This value corresponds to the isotope $^{85}$Rb for which $\Delta_0 = 3.0$ GHz. The isotope $^{87}$Rb, for which $\Delta_0 = 6.8$ GHz, in principle gives rise to an extra Stokes ring but with larger separation $\Delta\theta \simeq 0.37°$.
[41] B. Fazio, A. Irrera, S. Pirotta, C. D'Andrea, S. Del Sorbo, M. J. Lo Faro, P. G. Gucciardi, M. A. Iatì, R. Saija, M. Patrini, P. Musumeci, C. S. Vasi, D. S. Wiersma, M. Galli, and F. Priolo, Nat. Phot. **11**, 170 (2017).